

Optical properties of shock-compressed diamond up to 550 GPa

HPSTAR
940-2020Kento Katagiri^{1,*}, Norimasa Ozaki,^{1,2} Kohei Miyanishi³, Nobuki Kamimura,¹ Yuhei Umeda,¹ Takayoshi Sano²,
Toshimori Sekine,^{1,4} and Ryosuke Kodama^{1,2}¹Graduate School of Engineering, Osaka University, 2-1 Yamadaoka, Suita, Osaka 565-0871, Japan²Institute of Laser Engineering, Osaka University, 2-6 Yamadaoka, Suita, Osaka 565-0871, Japan³RIKEN SPring-8 Center, 1-1-1 Kouto, Sayo, Hyogo 679-5148, Japan⁴Center for High-Pressure Science and Technology Advanced Research, 1690 Cailun Rd., Pudong, Shanghai 201203, People's Republic of China

(Received 13 January 2020; revised manuscript received 26 March 2020; accepted 14 April 2020; published 11 May 2020)

A series of shock wave experiments were conducted to measure the optical properties of single-crystal diamond (100) in the pressure regime between 60 and 550 GPa. The results show that the transparency limit of diamond at 532 nm is ~ 170 GPa. When the applied pressure in diamond is lower than its Hugoniot elastic limit (HEL), diamond remains transparent during both compression and release processes. At the pressures between the HEL and the limit of its transparency, however, diamond is found to be transparent only while the compression is maintained and gradually loses its transparency during the subsequent release process. We also found that the refractive index of single-crystal diamond (100) monotonically increases as density increases to the limit of its transparency, in contrast to the previous static reports on continuous decrease of refractive index with increasing pressure up to 40 GPa.

DOI: [10.1103/PhysRevB.101.184106](https://doi.org/10.1103/PhysRevB.101.184106)

I. INTRODUCTION

Diamond is a unique material with mechanical, physical, and chemical properties such as highest hardness, small thermal expansion, high transparency, and high refractive index at ambient condition [1,2], although it is thermodynamically metastable. Since it is important to understand the high-pressure behaviors for various applications, the properties of diamond have been measured in a wide range of pressures [3–15]. However, the optical properties such as transparency and refractive index of diamond under pressure have not been fully elucidated.

The transparency of diamond under compression is controversial. According to the optical transmissivity model of diamond reported by Zhang *et al.* [16], diamond is transparent to the 532-nm probe light when the shock pressure is lower than 200 GPa. However, Yoo *et al.* found, during their shock experiments, that diamond (the type of diamond is not specified) is transparent in the entire pressure range to 300 GPa [17], while Bradley *et al.* and Coppari *et al.* indicated that single-crystal diamond (type not specified) is transparent up to 100 GPa under shock compression [3,18]. Lang and McWilliams *et al.*, however, noted that shocked single-crystal diamond (Lang used type IIa natural and synthetic diamond and McWilliams *et al.* used diamonds of type IIa, Ia, and Ib) is opaque over its Hugoniot elastic limit (HEL), which is lower than 100 GPa [4,5].

Refractive index is a fundamental property related to interatomic distance, electric polarizability, and band structure.

Changes in the refractive index under high pressure also provides information on high-energy optical transition and metallization [19]. Eremets *et al.* used diamond-anvil cell to measure the refractive index of diamond (type not specified) at pressures up to 40 GPa in the spectral range of 400–800 nm and found the refractive index of diamond decreases with increasing pressure to 40 GPa [6]. Later, Balzaretta and Jornada observed a similar behavior in natural diamond (type IIa) statically compressed up to 9 GPa [15]. In contrast to the static results, the linear photoelasticity theory predicts an increase in the refractive index with relatively small uniaxial strain along the (100) direction [20–22]. Lang found that the refractive indices of single-crystal diamond (type IIa) shock compressed along the directions of (100) and (111) increased with increasing the uniaxial stresses up to 90 GPa [4]. Lang also found that the linear photoelasticity theory is inaccurate under large uniaxial strain of shock compression, and experimentally determined the second-order elasto-optic constant from the nonlinear response of diamond under large uniaxial strain along the (100) direction.

The optical properties of transparent materials such as transparency and refractive index under pressure are particularly important for the usage of those materials as windows in dynamic compression experiments, as a transparent window attached on the rear surface of a sample can maintain pressure at the interface. Therefore, the *in situ* pressure state can be measured by recording the interface velocity using velocity interferometers such as line-imaging velocity interferometer systems for any reflector (VISAR) [23,24]. Thus, obtained velocity, termed as apparent particle velocity, is affected by the refractive index of shock-compressed window and differs from the true particle velocity of the reflector behind the

*Corresponding author: kkatagiri@ef.eie.eng.osaka-u.ac.jp

window. Therefore, precise measurements of the transparency and the refractive index of diamond as a function of shock pressure (or density) enable us to use diamond as an optical window for the velocity measurements in the dynamic compression experiments. Sapphire, lithium fluoride, and magnesium oxide are commonly accepted as optical windows for shock compression measurements [25–31], but none of them has a higher shock impedance than diamond. Thus, diamond window can synthesize a strong reflection wave back into the sample of interest to explore the high-pressure states with relatively low temperature, unless the shock impedance of the sample is lower than that of diamond [18,32].

II. EXPERIMENTAL METHODS

The experiments were performed at GEKKO XII laser facility (Institute of Laser Engineering, Osaka University). The wavelength of the 12 drive lasers in GEKKO XII was 527 or 351 nm, which is the second or the third harmonic wavelength of the neodymium glass laser with a fundamental wavelength of 1054 nm. The laser patterns were smoothed by using kinoform phase plates and the focal spot diameters on the target were 1000 and 600 μm for the second and third harmonic wavelengths, respectively. The duration of the laser pulses was 2.5 ns in the full width at half maximum with around 100 ps each for the rise and fall times. To deduce pressures in diamond, two VISAR systems with the 532-nm probe light were utilized to measure the velocity profiles. The velocity sensitivities of the VISARs were 2.240 and 1.356 km/s/fringe or 7.395 and 4.473 km/s/fringe. The VISAR data had a spatial resolution of $\sim 6 \mu\text{m}$ and a temporal resolution of ~ 100 ps, and the experimental uncertainties of velocities were less than 5% of the apparent velocity sensitivities.

The target configuration is presented in Fig. 1. The single-crystal diamond samples used in this work were synthesized by chemical vapor deposition at EDP Corporation and speci-

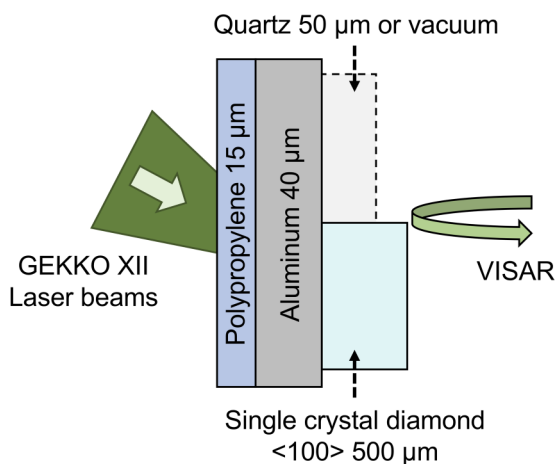


FIG. 1. Typical experimental setup of target consisting of polypropylene, aluminum, and single-crystal diamond $\langle 100 \rangle$. For some shots, an antireflection coated z-cut α -quartz was also on the rear surface of aluminum next to the diamond sample as a pressure standard. The thicknesses of polypropylene, aluminum, diamond, and quartz were 15, 40, 500, and 50 μm , respectively.

fied as type IIa. The initial density of single-crystal diamond is known to be 3.515 g/cm³ [1]. The diamond samples were $\sim 500 \mu\text{m}$ thick and 3×3 mm squares, and both surfaces were polished to achieve the surface roughness of less than 2 nm. The VISAR irradiation side was antireflection coated for 532 nm. The glue thickness between aluminum and diamond was measured to be less than 1 μm for each target.

According to the previous reports [3,7], the shock front of diamond does not become reflective at pressures below 500 GPa. Thus, all velocity profiles obtained in this work represent the apparent particle velocity from the aluminum-diamond interface through the shock-compressed diamond.

In this study, it is assumed that the shock wave is a single wave in diamond at pressures below 90 GPa, which is the HEL of single-crystal diamond $\langle 100 \rangle$ [4], and the elastic-plastic two-wave structure forms at higher pressure. The shock-compressed states of diamond were determined from using the known Hugoniot of single-crystal diamond $\langle 100 \rangle$ [4,33] and aluminum [34]. The Hugoniot of diamond has been precisely measured over 600 GPa [9–12] but only a few have been done to clarify the Hugoniot at lower pressures where diamond is not reflective [4,5,8,13,14]. In the present work, the elastic Hugoniot ($D_e = 17.52 + 0.755 U_e$) of single-crystal diamond $\langle 100 \rangle$ measured by Lang [4] and the plastic Hugoniot ($D_p = 11.76 + 1.056 U_p$) determined from the density functional theory calculation results reported by Romero and Mattson [33] were applied to obtain the shock-compressed state of diamond below and above the HEL, respectively. Here, D and U are the shock velocity and particle velocity, respectively. The subscripts e and p denote the elastic and plastic states, respectively. We note that the Hugoniot calculated by Romero and Mattson [33] is in broad agreement with several experimental data including the results from Pavlovskii [13], Kondo and Ahrens [14], and McWilliams *et al.* [5].

When a quartz witness was used on the rear surface of aluminum, the shock state of aluminum was determined from the known Hugoniot of aluminum and quartz [34] and the measured shock wave velocity of quartz, D_{qz} . The D_{qz} at pressures in quartz over 100 GPa [35] can be measured directly by VISAR due to its high reflectivity. For relatively low-pressure shots, we did not use a quartz witness and measured the free surface velocity of aluminum directly. In this case, the particle velocity of aluminum U_{Al} (km/s) was calculated from the measured free surface velocity of aluminum $U_{fs,Al}$ via $U_{fs,Al} = 0.046 U_{Al}^2 + 2.10 U_{Al} - 0.29$ (km/s), which is determined from known isentropic expansion data of aluminum [36–38].

III. RESULTS AND DISCUSSION

A. Transparency

Typical profiles of VISAR signal counts at three different pressures are shown as a function of time in Fig. 2. The results at pressures below 171 (± 12) GPa show that diamond remains transparent. For the relatively low pressure shocks where diamond remains transparent under compression, signal count is reduced by $\sim 30\%$ between 0 and 1 ns. This is due to the reflectivity change in aluminum by shock passage. After the drastic change in reflectivity from aluminum is

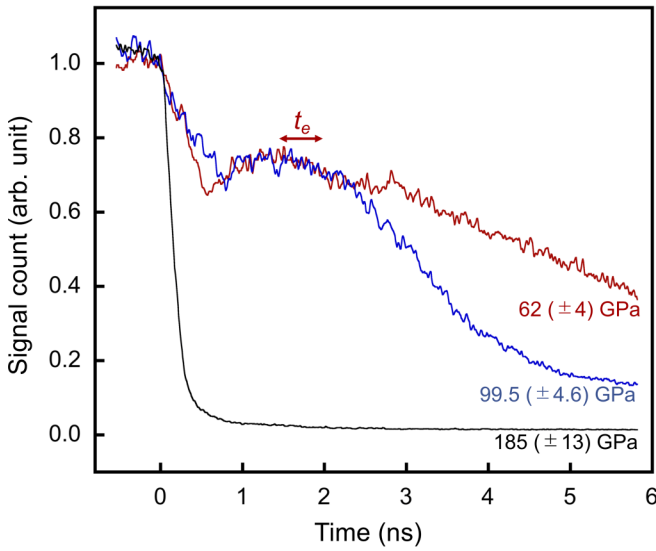


FIG. 2. Typical VISAR signal count profiles at three pressures. Time (t) zero is set when the shock wave breaks into the diamond from the aluminum. The signal count is normalized by the count at $t = 0$. The attenuation coefficient was calculated from the attenuation of the signal counts during the time, t_e , which is presented by a red two-direction arrow for the $62 (\pm 4)$ GPa shot.

stabilized, the signal counts begin to gradually decrease over time due to the attenuation of the probe light by diamond under pressure. At 2.5 ns, the rarefaction wave from the drive laser irradiation side starts propagation to release the pressure in the diamond sample. Below $77.0 (\pm 5.1)$ GPa, diamond remained transparent both in the processes of compression and release. At pressures between $99.5 (\pm 4.6)$ GPa and $171 (\pm 12)$ GPa, however, diamond was transparent only during the compression process and gradually became opaque during the subsequent release process. At pressures greater than $171 (\pm 12)$ GPa, diamond turned opaque during the compression process and the optical measurements through compressed diamond could not be obtained.

Since the VISAR signal count profiles presented in Fig. 2 indicate the reflectivity from aluminum through shock-compressed diamond, we can determine the pressure dependence of the attenuation coefficient in diamond to evaluate the transparency at high pressures. For the shots at pressures lower than HEL, the attenuation coefficient behind the elastic shock front α_e is calculated through

$$\alpha_e = -\frac{1}{2x_e} \ln \frac{I}{I_0}, \quad (1)$$

where x_e denotes the distance of elastic shock wave propagation, and I_0 and I are the signal counts before and after the shock wave propagates the distance of x_e , respectively [see Fig. 3(a)]. I_0 was taken at the time that the reflectivity of aluminum is stabilized [e.g., at 0.1 ns for the $185 (\pm 13)$ GPa shot and at 1.5 ns for the other two shots in Fig. 2]. We calculated α_e when the distance of the elastic shock wave propagation x_e is $10 \mu\text{m}$ where the shock remains steady, and the duration t_e is time for the shock wave with the speed D_e to travel the distance of the x_e , thus $t_e = x_e/D_e$. The t_e obtained

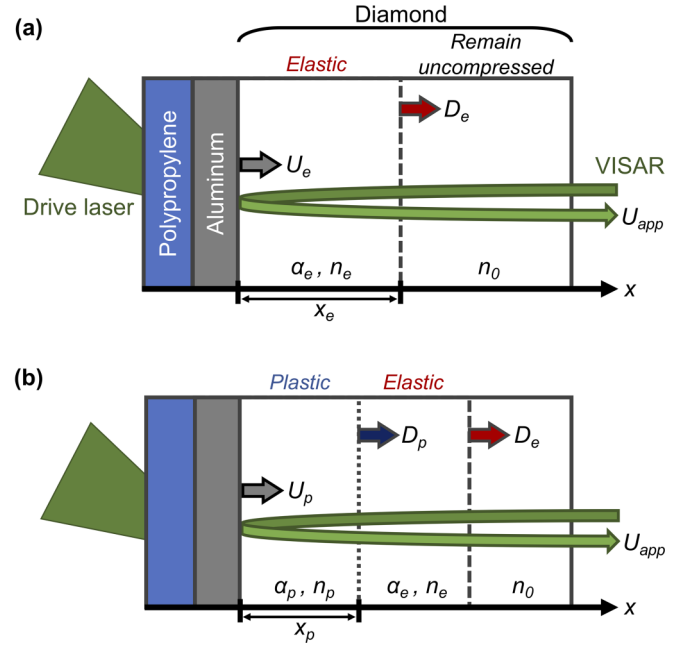


FIG. 3. VISAR measurements of apparent particle velocities from the aluminum-diamond interface through (a) purely elastic compression of diamond and (b) elastic-plastic compression of diamond. The shock front of diamond does not become reflective in our pressure range.

for the $62 (\pm 4)$ GPa shot is denoted by a red two-direction arrow in Fig. 2.

When the determined peak pressure in diamond is higher than the HEL of diamond, Eq. (2) was used instead of Eq. (1) to have the attenuation coefficient behind the plastic shock front, α_p :

$$\alpha_p = -\frac{1}{2x_p} \ln \frac{I}{I_0} - \alpha_e \frac{D_e - D_p}{D_p}. \quad (2)$$

We calculated α_p when the distance of the plastic shock wave propagation x_p is $10 \mu\text{m}$ [see Fig. 3(b)]. The constant value of $\alpha_e = 15 (\pm 1) \text{cm}^{-1}$, obtained from the data of purely elastic responses, is used. When D_p is faster than D_e , D_e becomes equal to D_p .

The estimated attenuation coefficient of diamond at 532 nm is presented as a function of shock pressure in Fig. 4. Diamond is opaque to 532-nm probe light at shock pressures over 170 GPa. This is explained by the effect of scattering from the plastically deformed diamond lattice. When the applied pressure exceeds the HEL, single-crystal diamond deforms plastically, possibly accompanying the polycrystallization process, to release the shear stress in the lattice. The probe light is unlikely to scatter back to its incident angle direction because the created grain boundaries in plastically deformed diamond are preferred to be along the (111) plane, which is the slip plane of diamond [5], while the incident angle of the probe light was perpendicular to the (100) planes of diamond in our experiments.

The experimentally determined transparency limit in shock-compressed diamond is 170 GPa and it differs from the optical transmissivity model by Zhang *et al.*, which reported

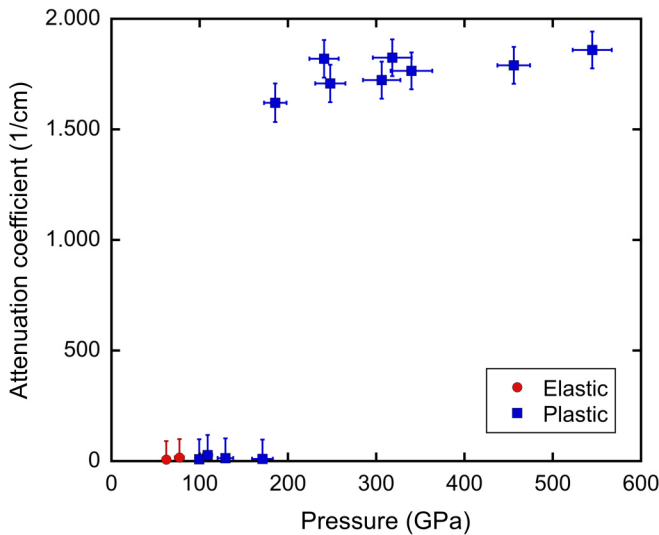


FIG. 4. Attenuation coefficients at 532 nm versus pressure measured for shocked single-crystal diamond $\langle 100 \rangle$. The red and blue symbols denote the elastic and plastic regions, respectively.

that diamond is transparent at shock pressure lower than 200 GPa [16]. This difference might be explained by the impurities in the diamond sample used in the present work, which can lower the pressure threshold for grain refining. We also note that our results showed a sharp decrease in transparency at around 170 GPa, while their transmissivity model predicted that the decrease in transparency would be more gradual [16].

At shock pressures between 90 and 170 GPa, we found that diamond was transparent during the compression process, then gradually turned opaque during the subsequent release process. The release process is caused by the propagation of rarefaction waves and is inevitable in dynamic compression experiments. The results indicate that the creation of grain boundaries in a shocked diamond is activated by the tensile stress during the release, even though the nucleation of the defects to cause the polycrystallization is thought to be already initiated during the compression. At pressures higher than 170 GPa, those defects would be directly formed and grown to cause the polycrystallization during the compression process, resulting in diamond becoming opaque at the early stage of shock propagation. When the applied pressure in diamond is lower than 90 GPa, which is the known HEL of single-crystal diamond $\langle 100 \rangle$ [4], diamond remained transparent during both the compression and release process.

B. Refractive index

The relationship between the apparent particle velocity (U_{app}) and the true particle velocity (U_e and U_p for elastic wave and plastic wave, respectively) of shock-compressed diamond is shown in Fig. 5. The linear fits for the relationship are expressed by $U_{app} = 2.14 (\pm 0.02) U_e$ and $U_{app} = 0.75 (\pm 0.19) + 1.64 (\pm 0.09) U_p$, for the elastic region (red line) and plastic region (blue line), respectively.

As Hardesty [39] and Setchell [25] expressed, the refractive index of material under purely elastic compression n_e is

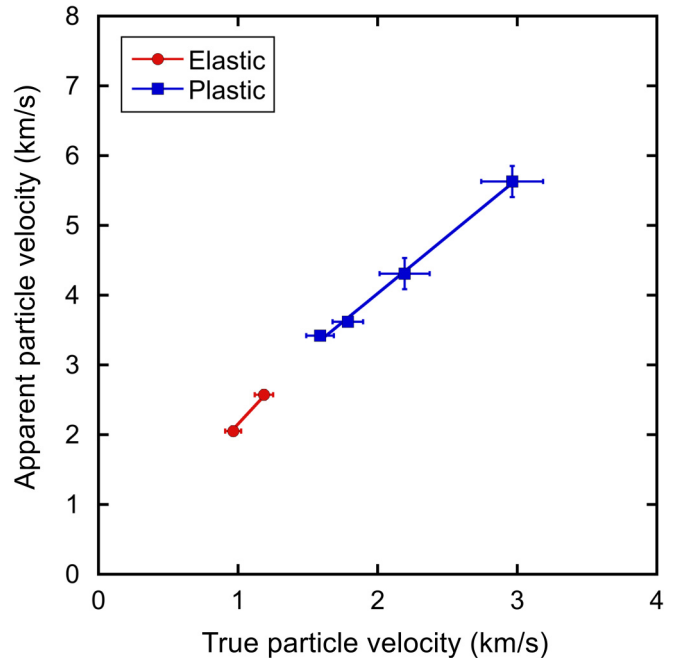


FIG. 5. Apparent particle velocity versus true particle velocity of single-crystal diamond $\langle 100 \rangle$ at 532 nm. The red and blue symbols denote the elastic and plastic regions, respectively.

defined as

$$n_e = \frac{U_{app} - D_e n_0}{U_e - D_e}. \quad (3)$$

Here, n_0 is the refractive index of an uncompressed sample [Fig. 3(a)]. However, as discussed by Fratanduono *et al.* [31], Eq. (3) is no longer valid when elastic-plastic two-wave structure within the sample [Fig. 3(b)] and, instead, the refractive index behind the plastic shock front n_p can be written as

$$n_p = \frac{U_{app} + (D_e - D_p)n_e - D_e n_0}{U_p - D_p}. \quad (4)$$

To determine n_p , the refractive index behind the preceding elastic wave is assumed to be a constant value of $n_e = 2.46$ [4].

The relationship between the refractive index (n_e and n_p for elastic wave and plastic wave, respectively) and the density (ρ) of shock-compressed single-crystal diamond $\langle 100 \rangle$ is shown in Fig. 6. The linear fits for the relationship are expressed by $n_e = 2.14 (\pm 0.04) + 0.08 (\pm 0.01) \rho$ and $n_p = 1.62 (\pm 0.07) + 0.22 (\pm 0.02) \rho$ for the elastic region with the ambient data [2] (red line) and the plastic region (blue line), respectively. The elastic results in this work concur with the elastic data of gas-gun experiments reported by Lang [4], which were measured to shock stresses between 60 and 90 GPa, using both synthetic and natural diamond crystals. The determined shock compression data and refractive index of single-crystal diamond $\langle 100 \rangle$ are listed in Table I.

The results show that the refractive index of shock-compressed diamond monotonically increases with increasing density up to a shock pressure of $171 (\pm 12)$ GPa [equivalent to the shock density of $4.30 (\pm 0.13) \text{ g/cm}^3$], which is the limit of its transparency. Our results are consistent with the

TABLE I. Summary of the shock compression data.

Experiment number	Free surface velocity of aluminum $U_{fs,Al}$ (km/s)	Shock wave velocity of quartz D_{qz} (km/s)	True particle velocity U (km/s)	Apparent particle velocity U_{app} (km/s)	Shock pressure P (GPa)	Density ρ (g/cm^3)	Refractive index n
42192 ^a	3.62 ± 0.07		0.97 ± 0.07	2.05 ± 0.07	62 ± 4	3.71 ± 0.06	2.44 ± 0.04
42189 ^a	4.35 ± 0.07		1.19 ± 0.08	2.57 ± 0.07	77.0 ± 5.1	3.76 ± 0.06	2.44 ± 0.04
42190	5.48 ± 0.07		1.59 ± 0.10	3.42 ± 0.07	99.5 ± 4.6	3.86 ± 0.06	2.45 ± 0.05
42191	5.98 ± 0.07		1.79 ± 0.11	3.62 ± 0.07	109 ± 5	3.93 ± 0.07	2.47 ± 0.05
42316	7.01 ± 0.22		2.20 ± 0.18	4.31 ± 0.22	129 ± 9	4.06 ± 0.10	2.50 ± 0.08
42903	9.00 ± 0.22		2.96 ± 0.22	5.63 ± 0.22	171 ± 12	4.30 ± 0.13	2.55 ± 0.09
42894 ^b	9.65 ± 0.22		3.21 ± 0.24		185 ± 13	4.38 ± 0.14	
42182 ^b	11.98 ± 0.22		4.08 ± 0.28		240 ± 17	4.66 ± 0.17	
42194 ^b	12.27 ± 0.22		4.19 ± 0.29		247 ± 17	4.69 ± 0.17	
42179 ^b	14.53 ± 0.22		5.01 ± 0.33		305 ± 21	4.95 ± 0.21	
42175 ^b	14.98 ± 0.22		5.17 ± 0.33		317 ± 22	5.00 ± 0.21	
42173 ^b	15.78 ± 0.22		5.46 ± 0.35		339 ± 23	5.09 ± 0.23	
42171 ^{b,c}		15.38 ± 0.15	6.85 ± 0.20		455 ± 18	5.51 ± 0.15	
42167 ^{b,c}		16.81 ± 0.15	7.81 ± 0.22		543 ± 22	5.81 ± 0.17	

^aResults below the HEL.

^bDiamond was opaque to the 532-nm probe light.

^cQuartz witness was used.

nonlinear photoelasticity theory that predicts the increase in the refractive index under large uniaxial strain in single-crystal diamond elastically compressed along the $\langle 100 \rangle$ orientation up to 90 GPa [4]. Eremets *et al.*, however, reported that the refractive index of statically compressed diamond decreased monotonically from the ambient value with increasing pressure up to 40 GPa [6]. As explained by Lang, this difference in optical tendency suggests that the anisotropy of deformation strongly affects the optical response of diamond

[4]. Notably, the refractive index of diamond shocked along $\langle 100 \rangle$ increases with increasing density even over its HEL, where diamond deforms plastically. High-accuracy measurements of flyer impact experiments and theoretical works are expected for a deeper understanding of the tendency of the refractive index of diamond over the HEL. We also found that the refractive index of shock-compressed magnesium oxide increases with increasing density over 6 g/cm^3 [40] in contrast to the monotonical decrease of the refractive index as the density increases at lower densities observed by Fratanduono *et al.* [31].

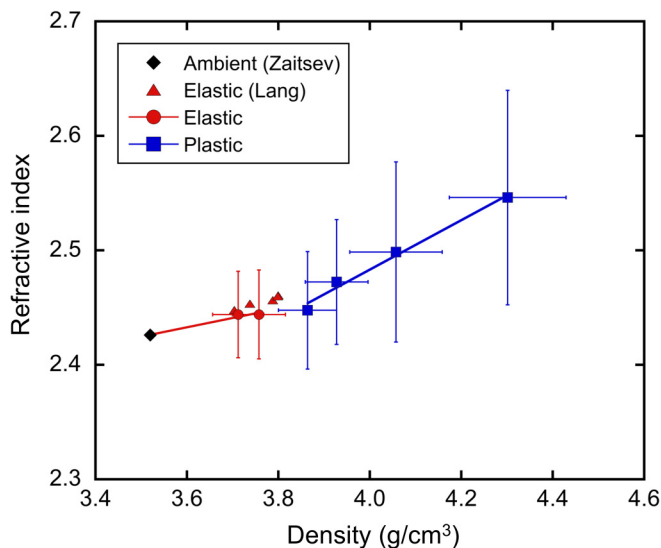


FIG. 6. Refractive index at 532 nm versus density of shocked single-crystal diamond $\langle 100 \rangle$. The symbols are the same as in Fig. 5. Black square and red triangles are the ambient value (Ref. [2]) and the data from elastic shock experiments using a gas gun (Ref. [4]), respectively.

IV. SUMMARY AND CONCLUSIONS

In this paper, we studied the transparency and the refractive index of single-crystal diamond $\langle 100 \rangle$ at 532 nm, under shock pressures between 60 and 550 GPa. These properties are important to develop diamond as the highest shock impedance window material for velocity measurements of dynamic compression experiments. When the shock pressure in diamond is lower than 170 GPa, diamond is found to be transparent, thus diamond can work as an optical window. The density dependence of the refractive index of diamond obtained in this study can be used to investigate the shock compression state of a material through a diamond window.

At shock pressures of 90–170 GPa, diamond is found to be transparent during the compression process, then gradually turns opaque during the subsequent release process. The results suggest that the polycrystallization process of a shocked diamond is largely different below and above 170 GPa. Understanding those polycrystallization mechanisms under shock loading would give insight into a field of material engineering to study material strengthening using laser refinement.

ACKNOWLEDGMENTS

We thank J. Lintz for valuable discussions. The experiments were conducted under the joint research of the Institute of Laser Engineering, Osaka University. This work was supported by grants from MEXT Quantum Leap Flagship

Program (MEXT Q-LEAP) Grant No. JPMXS0118067246, Japan Society for the Promotion of Science (JSPS) KAKENHI (Grants No. 19K21866 and No. 16H02246), and Genesis Research Institute, Inc. (Konpon-ken, Toyota). We also acknowledge partial support by HPSTAR, China.

-
- [1] J. E. Field, *The properties of natural and synthetic Ddiamond* (Academic, New York, 1992).
- [2] A. M. Zaitsev, *Optical properties of diamond: A data handbook* (Springer-Verlag, Berlin, Heidelberg, 2001).
- [3] D. K. Bradley, J. H. Eggert, D. G. Hicks, P. M. Celliers, S. J. Moon, R. C. Cauble, and G. W. Collins, Shock Compressing Diamond to a Conducting Fluid, *Phys. Rev. Lett.* **93**, 195506 (2004).
- [4] J. M. Lang, Ph.D. thesis, Washington State University, 2013.
- [5] R. S. McWilliams, J. H. Eggert, D. G. Hicks, D. K. Bradley, P. M. Celliers, D. K. Spaulding, T. R. Boehly, G. W. Collins, and R. Jeanloz, Strength effects in diamond under shock compression from 0.1 to 1 TPa, *Phys. Rev. B* **81**, 014111 (2010).
- [6] M. I. Eremets, V. V. Struzhkin, Ju. A. Timofeev, I. A. Trojan, A. N. Utjuzh, and A. M. Shirokov, Refractive index of diamond under pressure, *High Press. Res.* **9**, 347 (1992).
- [7] J. H. Eggert, D. G. Hicks, P. M. Celliers, D. K. Bradley, R. S. McWilliams, R. Jeanloz, J. E. Miller, T. R. Boehly, and G. W. Collins, Melting temperature of diamond at ultrahigh pressure, *Nat. Phys.* **6**, 40 (2010).
- [8] J. M. Lang and Y. M. Gupta, Experimental Determination of Third-Order Elastic Constants of Diamond, *Phys. Rev. Lett.* **106**, 125502 (2011).
- [9] H. Nagao, K. G. Nakamura, K. Kondo, N. Ozaki, K. Takamatsu, T. Ono, T. Shiota, D. Ichinose, K. A. Tanaka, K. Wakabayashi, K. Okada, M. Yoshida, M. Nakai, K. Nagai, K. Shigemori, T. Sakaiya, and K. Otani, Hugoniot measurement of diamond under laser shock compression up to 2 TPa, *Phys. Plasmas* **13**, 052705 (2006).
- [10] S. Brygoo, E. Henry, P. Loubeyre, J. H. Eggert, M. Koenig, B. Loupays, A. Benuzzi-Mounaix, and M. Rabec Le Gloahec, Laser-shock compression of diamond and evidence of a negative-slope melting curve, *Nat. Mater.* **6**, 274 (2007).
- [11] D. G. Hicks, T. R. Boehly, P. M. Celliers, D. K. Bradley, J. H. Eggert, R. S. McWilliams, R. Jeanloz, and G. W. Collins, High-precision measurements of the diamond Hugoniot in and above the melt region, *Phys. Rev. B* **78**, 174102 (2008).
- [12] M. D. Knudson, M. P. Desjarlais, and D. H. Dolan, Shock-wave exploration of the high-pressure phases of carbon, *Science* **322**, 1822 (2008).
- [13] M. N. Pavlovskii, Shock compression of diamond, *Sov. Phys. Solid State* **13**, 741 (1971).
- [14] K. Kondo and T. J. Ahrens, Shock compression of diamond crystal, *Geophys. Res. Lett.* **10**, 281 (1983).
- [15] N. M. Balzaretto and J. A. H. da Jornada, Pressure dependence of the refractive index of diamond, cubic silicon carbide and cubic boron nitride, *Solid State Commun.* **99**, 943 (2009).
- [16] Z. Zhang, Y. Zhao, and J. Yang, Transparency of the strong shock-compressed diamond for 532 nm laser light, *Phys. Plasmas* **23**, 043301 (2016).
- [17] C. S. Yoo, N. C. Holmes, and M. Ross, Shock Temperatures and Melting of Iron at Earth Core Conditions, *Phys. Rev. Lett.* **70**, 3931 (1993).
- [18] F. Coppari, R. F. Smith, J. H. Eggert, J. Wang, J. R. Rygg, A. Lazicki, J. A. Hawreliak, G. W. Collins, and T. S. Duffy, Experimental evidence for a phase transition in magnesium oxide at exoplanet pressures, *Nat. Geosci.* **6**, 926 (2013).
- [19] A. Dewaele, J. H. Eggert, P. Loubeyre, and R. Le Toullec, Measurement of refractive index and equation of state in dense He, H₂, H₂O, and Ne under high pressure in a diamond anvil cell, *Phys. Rev. B* **67**, 094112 (2003).
- [20] J. F. Nye, *Physical properties of crystals* (Clarendon, Oxford, 1957).
- [21] A. Yariv and P. Yev, *Optical waves in crystals* (Wiley, New York, 1984).
- [22] M. H. Grimsditch and A. K. Ramdas, Brillouin scattering in diamond, *Phys. Rev. B* **11**, 3139 (1975).
- [23] L. M. Barker and R. E. Hollenbach, Laser interferometer for measuring high velocities of any reflecting surface, *J. Appl. Phys.* **43**, 4669 (1972).
- [24] P. M. Celliers, D. K. Bradley, G. W. Collins, D. G. Hicks, T. R. Boehly, and W. J. Armstrong, Line-imaging velocimeter for shock diagnostics at the OMEGA laser facility, *Rev. Sci. Instrum.* **75**, 4916 (2004).
- [25] R. E. Setchell, Index of refraction of shock-compressed fused silica and sapphire, *J. Appl. Phys.* **50**, 8186 (1979).
- [26] R. E. Setchell, Refractive index of sapphire at 532 nm under shock compression and release, *J. Appl. Phys.* **91**, 2833 (2002).
- [27] X. Cao, Y. Wang, X. Li, L. Xu, L. Liu, Y. Yu, R. Qin, W. Zhu, S. Tang, L. He, C. Meng, B. Zhang, and X. Peng, Refractive index and phase transformation of sapphire under shock pressures up to 210 GPa, *J. Appl. Phys.* **121**, 115903 (2017).
- [28] D. Hayes, Unsteady compression waves in interferometer windows, *J. Appl. Phys.* **89**, 6484 (2001).
- [29] P. A. Rigg, M. D. Knudson, R. J. Scharff, and R. S. Hixson, Determining the refractive index of shocked [100]lithium fluoride to the limit of transmissivity, *J. Appl. Phys.* **116**, 033515 (2014).
- [30] G. Young, X. Liu, C. Leng, J. Yang, and H. Huang, Refractive index of [100] lithium fluoride under shock pressures up to 151 GPa, *AIP Adv.* **8**, 125310 (2018).
- [31] D. E. Fratanduono, J. H. Eggert, M. C. Akin, R. Chau, and N. C. Holmes, A novel approach to Hugoniot measurements utilizing transparent crystals, *J. Appl. Phys.* **114**, 043518 (2013).
- [32] M. Millot, F. Coppari, J. R. Rygg, A. C. Barrios, S. Hamel, D. C. Swift, and J. H. Eggert, Nanosecond X-ray diffraction of shock-compressed superionic water ice, *Nature (London)* **569**, 251–255 (2019).
- [33] N. A. Romero and W. D. Mattson, Density-functional calculation of the shock Hugoniot for diamond, *Phys. Rev. B* **76**, 214113 (2007).

- [34] M. D. Knudson and M. P. Desjarlais, Adiabatic release measurements in α -quartz as a shock standard in the multimegabar regime, *Phys. Rev. B* **88**, 184107 (2013).
- [35] M. D. Knudson and M. P. Desjarlais, Shock Compression of Quartz to 1.6 TPa: Redefining a Pressure Standard, *Phys. Rev. Lett.* **103**, 225501 (2009).
- [36] A. A. Bakanova, I. P. Dudoladov, M. V. Zhernokletov, V. N. Zubarev, and G. V. Simakov, Vaporization of shock-compressed metals on expansion, *J. Appl. Mech. Tech. Phys.* **24**, 204 (1983).
- [37] B. L. Glushak, A. P. Zharkov, M. V. Zhernokletov, V. Ya. Ternovoi, A. S. Filimonov, and V. E. Fortov, Experimental investigation of the thermodynamics of dense plasmas formed from metals at high energy concentrations, *Sov. Phys. JETP* **69**, 739 (1989).
- [38] M. V. Zhernokletov, G. V. Simakov, Yu. N. Sutulov, and R. F. Trunin, Expansion isentropes of aluminum, iron, molybdenum, lead, and tantalum, *High Temp.* **33**, 40 (1995).
- [39] D. R. Hardesty, On the index of refraction of shock-compressed liquid nitromethane, *J. Appl. Phys.* **47**, 1994 (1976).
- [40] K. Miyanishi (private communication).